

MODELING OF A SOLAR REACTOR FOR WATER PURIFICATION, EMPLOYING THE PHOTO-FENTON REACTION

Germán H. Rossetti, Enrique D. Albizzati,
and Orlando M. Alfano



Universidad Nacional del Litoral - CONICET
Güemes 3450, 3000 Santa Fe, Argentina
E-mail: alfano@intec.unl.edu.ar

OUTLINE

- x Introduction
- x Mass Balances
- x Kinetic Model
- x Radiation Field
- x Model Parameters and Numerical Solution
- x Predicted and Experimental Results
- x Effects of the Reaction Temperature
- x Final Remarks

INTRODUCTION

- × The Fenton reaction is a chemical system involving hydrogen peroxide and ferrous salts that generates highly reactive hydroxyl radicals.
- × The oxidation ability of the Fenton mixture can be greatly enhanced using UV (or UV/Vis) radiation: the photo-Fenton Reaction.
- In this work, the degradation of formic acid (a model pollutant) in aqueous solution using the Fenton and photo-Fenton systems is presented.
- The reaction was conducted in a flat-plate solar reactor placed inside the loop of a batch recycling system.

INTRODUCTION: PREVIOUS WORK

Modeling and Experimental
Verification of a Flat-Plate Solar

Photoreactor
Reactor

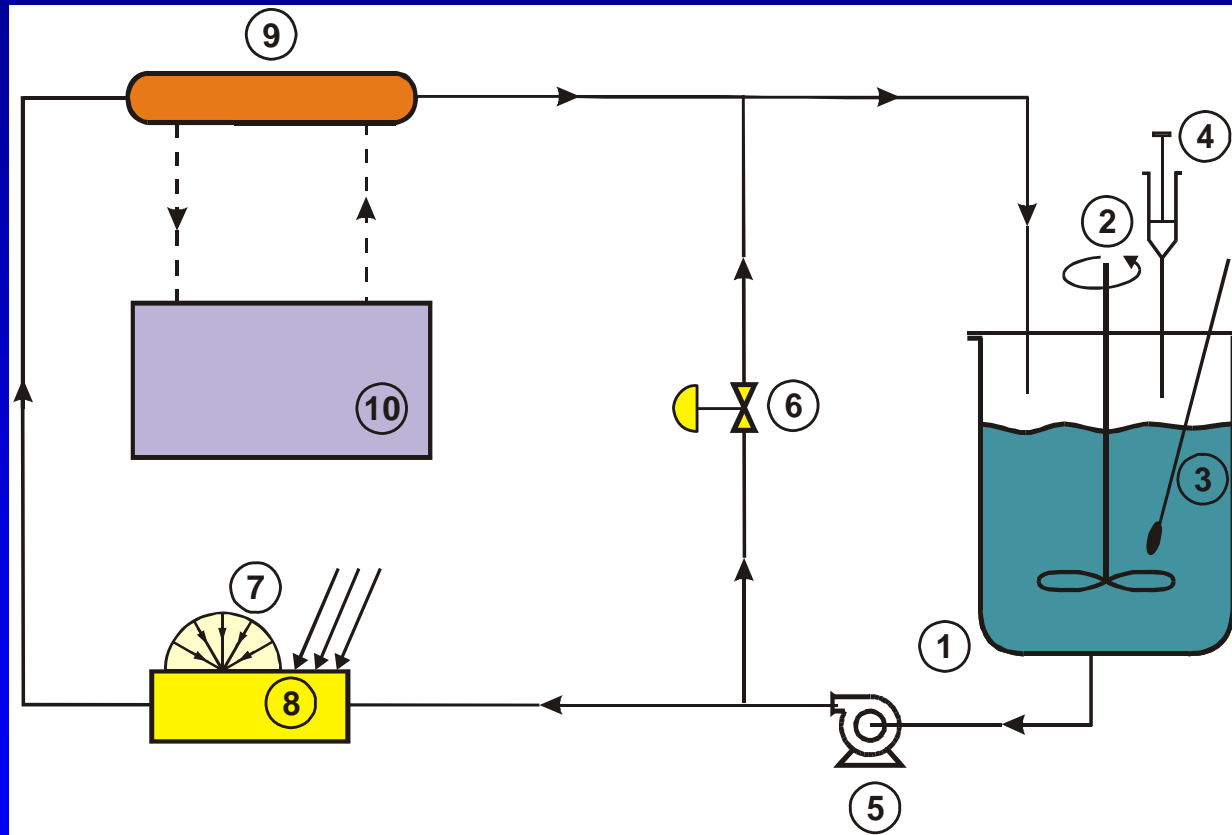
Decomposition of Formic Acid in a
Water Solution Employing the
Photo-Fenton Reaction, Ind. Eng.

Chem.

Modeling of a Flat-Plate Solar
Reactor. Degradation of Formic Acid
by the Photo-Fenton Reaction, Solar

Temperature Effects on the Photo-Fenton
Degradation of Formic Acid, ENPROMER 2005,
Río de Janeiro, Brasil; III EPOA, Campinas, Brasil.

FLOW SHEET OF THE EXPERIMENTAL DEVICE

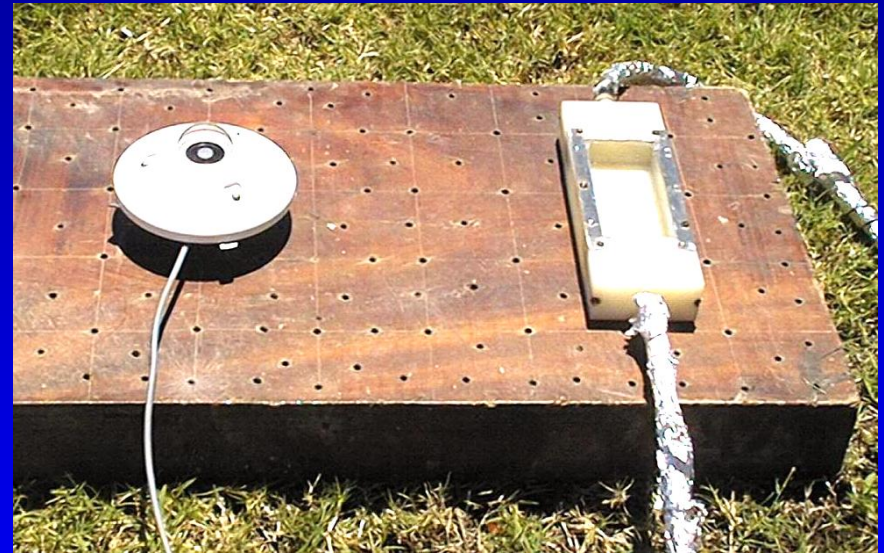


Keys: (1) storage tank, (2) stirrer, (3) thermometer, (4) liquid sampling, (5) pump, (6) valve, (7) solar radiation, (8) flat-plate reactor, (9) heat exchanger, and (10) thermostatic bath.

PICTURE OF THE EXPERIMENTAL DEVICE




- x Well-stirred batch recycling photoreactor



- x Flat-plate solar reactor
- x Broadband UV Radiometer CUV3 of Kipp & Zonen

OUTLINE

- x Introduction
-  x **Mass Balances**
- x Kinetic Model
- x Radiation Field
- x Model Parameters and Numerical Solution
- x Predicted and Experimental Results
- x Effects of the Reaction Temperature
- x Final Remarks

MASS BALANCES (F: formic acid; P: Hydrogen Peroxide)

$$\frac{dC_F}{dt} = \frac{V_R}{V_T} \langle R_F(\mathbf{x}, t) \rangle_{V_R} + \left(\frac{V_{Tk}}{V_T} \right) R_F^t(t)$$

photo-Fenton

Fenton

$$\frac{dC_P}{dt} = \frac{V_R}{V_T} \langle R_P(\mathbf{x}, t) \rangle_{V_R} + \left(\frac{V_{Tk}}{V_T} \right) R_P^t(t)$$

photo-Fenton

Fenton

Initial conditions:

$$t = 0 \quad C_F = C_F^0$$

$$t = 0 \quad C_P = C_P^0$$

× V_R/V_T for photo-Fenton

× V_{Tk}/V_T for Fenton

× The average value must

be retained in order to

account for spatial

variations of the photo-

Fenton reaction rate


× Spatial variations of the

Local Volumetric Rate

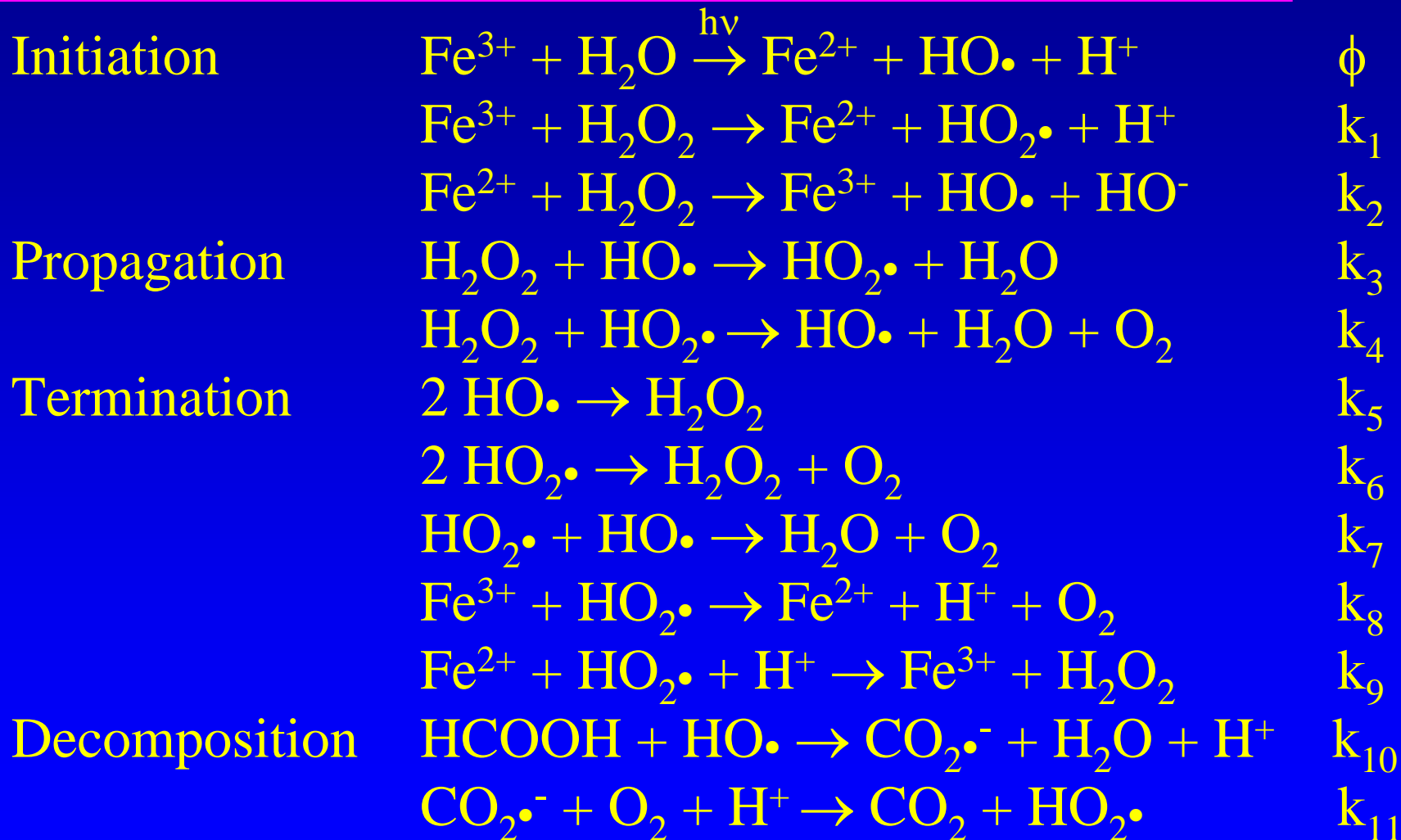
of Photon Absorption

(LVRPA)

OUTLINE

- x Introduction
- x Mass Balances
-  x **Kinetic Model**
- x Radiation Field
- x Model Parameters and Numerical Solution
- x Predicted and Experimental Results
- x Effects of the Reaction Temperature
- x Final Remarks

REACTION SCHEME^(*)



(*) Proposed by Pignatello (1992), De Laat and Gallard (1999)

ASSUMPTIONS FOR THE KINETIC MODEL

The following assumptions have been considered:

- x the steady state approximation (SSA) may be applied for highly reactive radicals, such as $\text{OH}\cdot$ and $\text{HO}_2\cdot$,
- x radical-radical termination reactions are neglected as compared with the propagation reactions,
- x the ferrous ion concentration remains constant during the reaction time,
- x the oxygen concentration is always in excess.

KINETIC MODEL

$$R_F(\underline{x}, t) = - \left(\frac{\bar{\Phi} \sum e_{\lambda}^a(\underline{x}, t)}{\lambda} \right) + \left(1 + \frac{\bar{\Phi} \sum e_{\lambda}^a(\underline{x}, t)}{\lambda} \right)^{1/2} R_F^t(t)$$

$\bar{\Phi}$: wavelength-averaged primary quantum yield

$e_{\lambda}^a(\underline{x}, t)$: spectral LVRPA

K_i : kinetic parameters ($i = 1$ to 4)

When $\sum_{\lambda} e^a(\underline{x}, t) = 0$, the pollutant reaction rate is not null. A thermal reaction rate can be identified (Fenton reaction).

This term may be represented by the expression:

$$R_F^t(t) = -K_1 \frac{1 + K_2 (C_P / C_{Fe^{3+}})}{1 + K_3 (C_P / C_F)} C_{Fe^{3+}} C_P$$

OUTLINE

x Introduction

x Mass Balances

x Kinetic Model



x **Radiation Field**

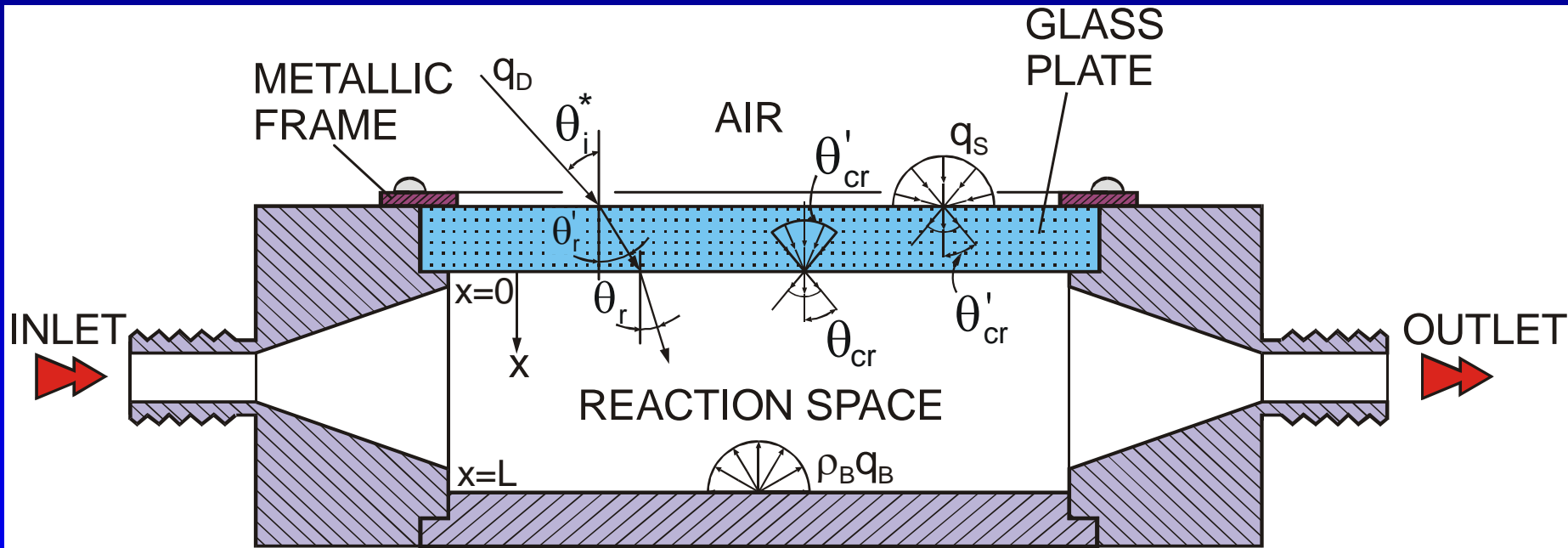
x Model Parameters and Numerical Solution

x Predicted and Experimental Results

x Effects of the Reaction Temperature

x Final Remarks

RADIATION FIELD MODELING



- × Schematic representation of the flat-plate solar reactor
- × At the top, a window made of glass was located
- × The surface of radiation entrance receives direct solar radiation (q_D) and diffuse solar radiation (q_S)

RADIATION FIELD MODELING

Radiative Transfer Equation:

$$\mu \frac{\partial I_\lambda(x, \mu, \phi)}{\partial x} + \kappa_\lambda I_\lambda(x, \mu, \phi) = 0$$

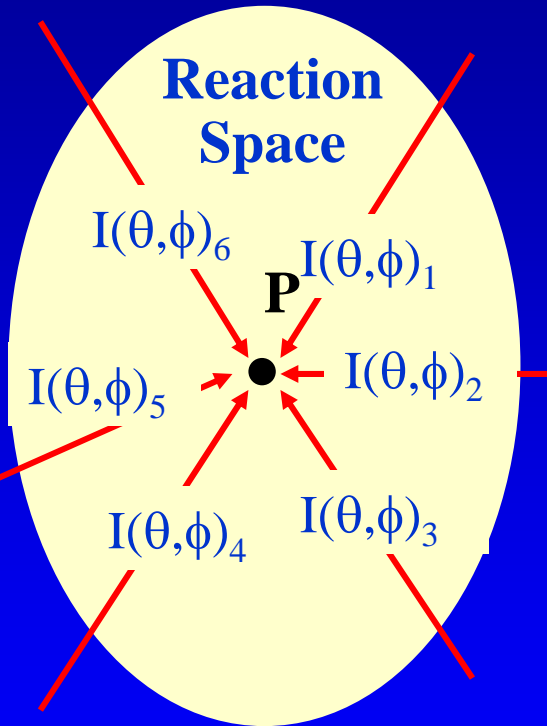
$$\mu = \cos \theta$$

Variation of the Radiation Intensity along the ray path

Radiation absorption

- B.C. at $x = 0$: (i) reflection and refraction at the interfaces and (ii) radiation absorption inside the glass window
- B.C. at $x = L$: radiation intensity reaching the reactor bottom is reflected back to the solution in a diffuse manner

EVALUATION OF THE LVRPA



Once the radiation intensity $I_\lambda(\mathbf{x}, \mu, \phi)$ is obtained, one can compute the LVRPA:

- × Radiation may be arriving at one point (P) inside the reaction space from all directions in space
- × An integration over all the arriving rays (θ, ϕ) is required:

$$e_\lambda^a(\mathbf{x}) = \kappa_\lambda \int_0^{2\pi} d\phi \int_{-1}^1 I_\lambda(\mathbf{x}, \mu, \phi) d\mu$$

Integrating the previous equation, LVRPA is obtained:

FINAL EXPRESSION OF THE LVRPA

$$e_{\lambda}^a(x) = \kappa_{\lambda} \left\{ q_{D,\lambda} \frac{[1 - \rho_{a-p}(\mu_i^*)][1 - \rho_{p-w}(\mu'_r)]\tau_{\lambda}(\mu'_r)}{1 - \tau_{\lambda}^2(\mu'_r)\rho_{a-p}(\mu'_r)\rho_{p-w}(\mu'_r)} \exp(-\kappa_{\lambda} x / \mu_r) + \right.$$



Direct solar radiation

$$2q_{S,\lambda} \frac{n_w^2}{n_a^2} \int_{\mu_{cr}}^1 \frac{[1 - \rho_{a-p}(\mu^*)][1 - \rho_{p-w}(\mu')]\tau_{\lambda}(\mu')}{1 - \tau_{\lambda}^2(\mu')\rho_{a-p}(\mu')\rho_{p-w}(\mu')} \exp(-\kappa_{\lambda} x / \mu) d\mu +$$




Diffuse solar radiation

$$2\rho_B q_{B,\lambda} \left[\int_0^1 \rho_{w-p}(\mu) \exp[-\kappa_{\lambda} (L + x) / \mu] d\mu + \int_0^1 \exp[-\kappa_{\lambda} (L - x) / \mu] d\mu \right]$$

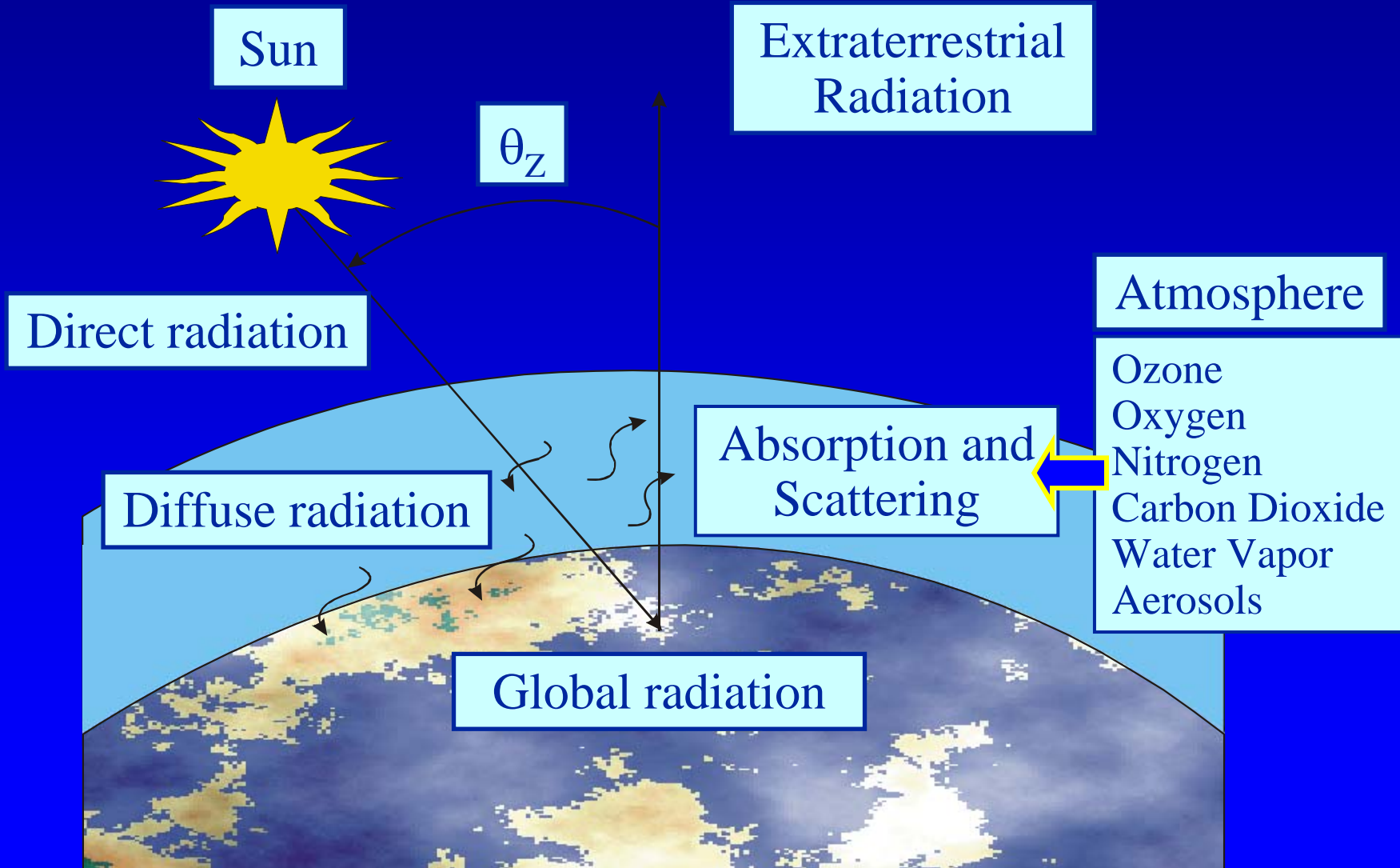


Radiation flux at the reactor bottom

OUTLINE

- x Introduction
- x Mass Balances
- x Kinetic Model
- x Radiation Field
-  x **Model Parameters and Numerical Solution**
- x Predicted and Experimental Results
- x Effects of the Reaction Temperature
- x Final Remarks

SOLAR RADIATION INCIDENT AT THE REACTOR WINDOW



SOLAR RADIATION INCIDENT AT THE REACTOR WINDOW

→ Global radiation on a horizontal surface at ground level for wavelength λ (Bird and Riordan, 1986):

$$q_{G,\lambda} = q_{D,\lambda} \cos \theta_Z + q_{S,\lambda} \quad (\theta_Z = \text{zenith angle})$$

× Direct radiation on a surface normal to the sun direction:

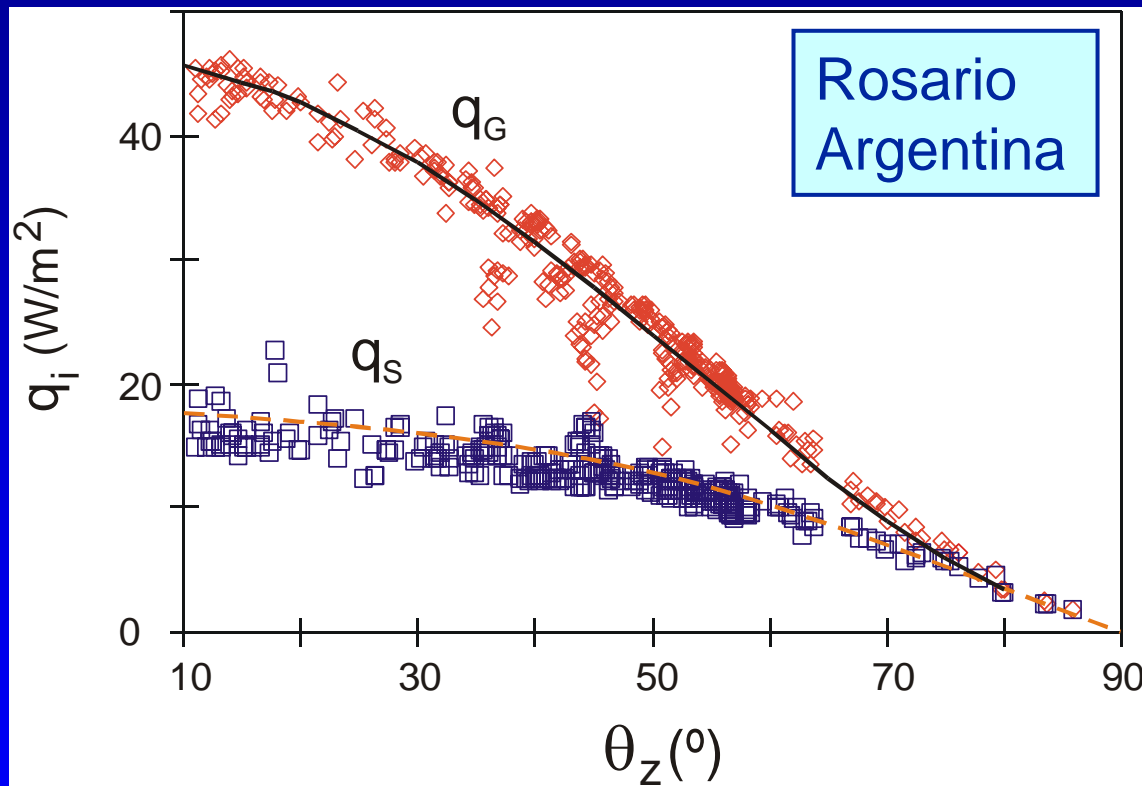
$$q_{D,\lambda} = H_{0,\lambda} D T_{r,\lambda} T_{a,\lambda} T_{w,\lambda} T_{o,\lambda} T_{u,\lambda}$$

× Diffuse radiation on a horizontal surface at ground level:

$$q_{S,\lambda} = q_{r,\lambda} + q_{a,\lambda} + q_{g,\lambda}$$

where: Rayleigh scattering ($q_{r,\lambda}$), aerosol scattering ($q_{a,\lambda}$), multiple reflection of radiation between the ground and the air ($q_{g,\lambda}$)

GLOBAL AND DIFFUSE UV SOLAR RADIATION



× Measurements and model predictions:

- horizontal surface
- clear sky days

× Model predictions:

- Global (—)
- Diffuse (- - -)

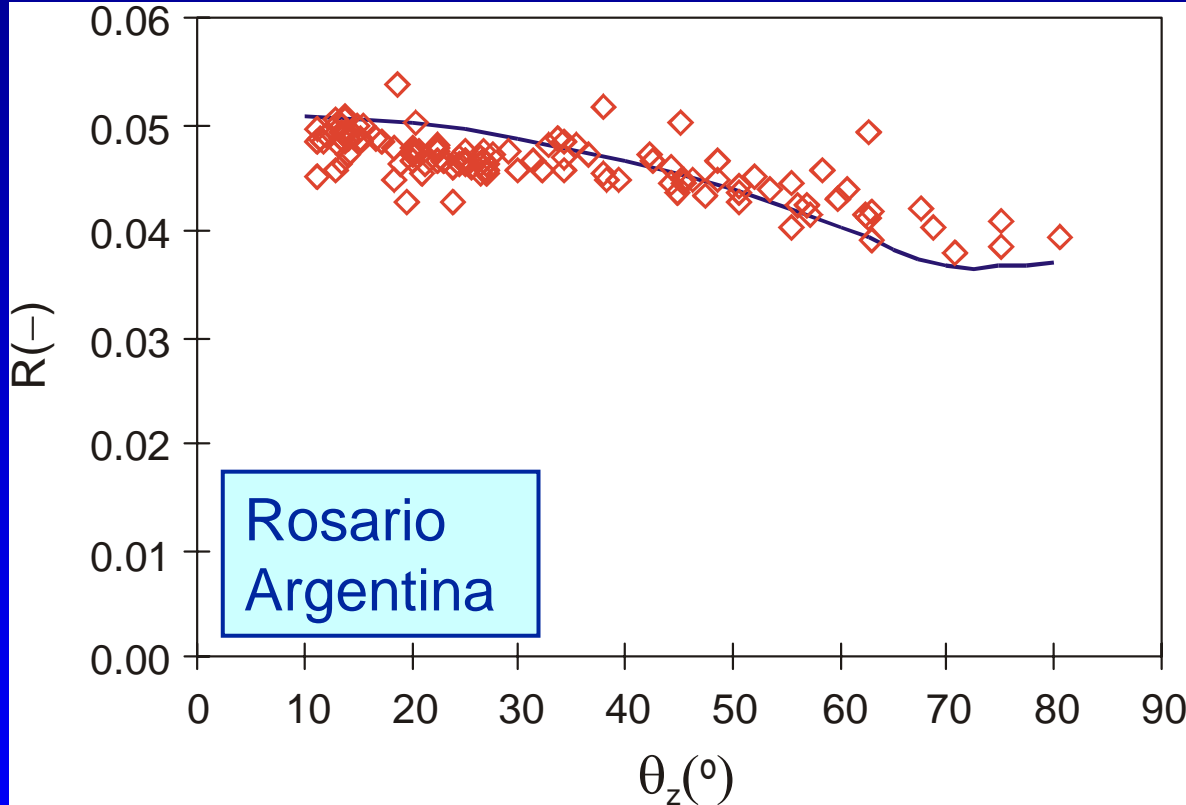
× Measurements:

- Global (\diamond)
- Diffuse (\square)

× Maximum UV solar radiation: $q_{G,max} \cong 45 W/m^2$

× At $\theta_z > 45^\circ \rightarrow$ Diffuse radiation $>$ Direct radiation

RATIO OF UV TO TOTAL SOLAR RADIATION (R)

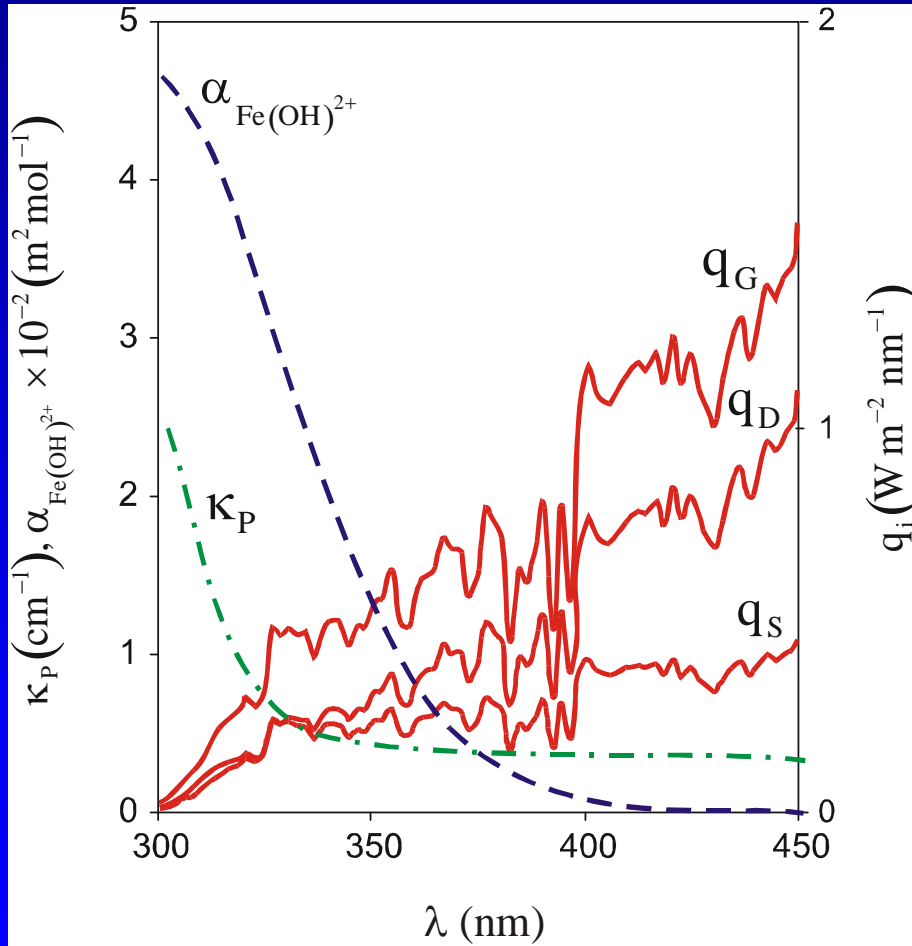


Measurements (\diamond)
and predictions (—):
 \Rightarrow horizontal surface
 \Rightarrow clear sky days

$\theta_z(^{\circ})$	R%
12	5.2
20	5.1
40	4.8
60	4.2
80	3.9

- x UV solar radiation: 4 to 5% of the total solar radiation
- x R decreases when the zenith angle is increased

SPECTRAL DATA



- ✘ Global (q_G), direct (q_D) and diffuse (q_S) solar radiation (Bird and Riordan, 1986) for:
 - cloudless sky conditions
 - solar zenith angle = 10°
- ✘ Molar absorptivity of the iron complex: $\alpha_{\text{Fe}(\text{OH})^{2+}}$
- ✘ Absorption coefficient of the glass plate: κ_P

NUMERICAL SOLUTION: COMPUTATIONAL STEPS

Evaluation of the direct and diffuse solar radiation incident at the reactor


Computation of the LVRPA as a function of position

Evaluation of the formic acid and hydrogen peroxide

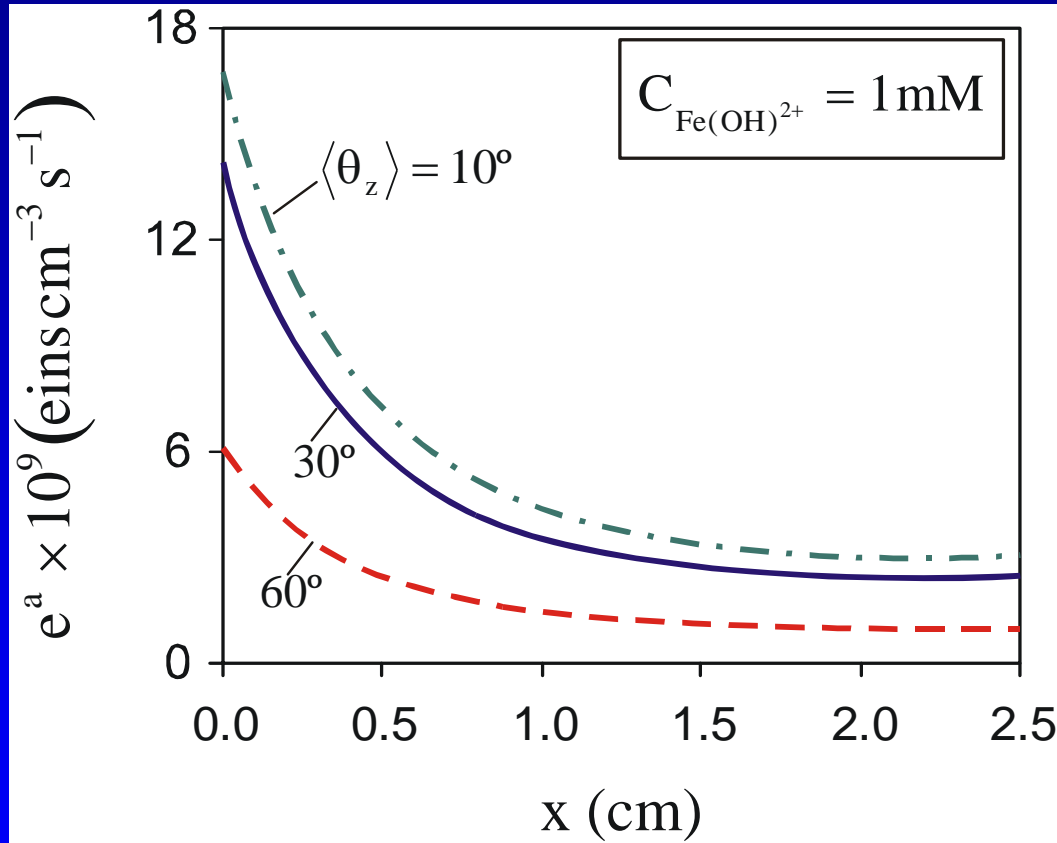
Calculation of the formic acid and hydrogen peroxide concentrations as a function of time

System of two nonlinear, first order, ordinary differential equations

OUTLINE

- x Introduction
- x Mass Balances
- x Kinetic Model
- x Radiation Field
- x Model Parameters and Numerical Solution
-  x **Predicted and Experimental Results**
- x Effects of the Reaction Temperature
- x Final Remarks

PREDICTIONS OF THE LVRPA

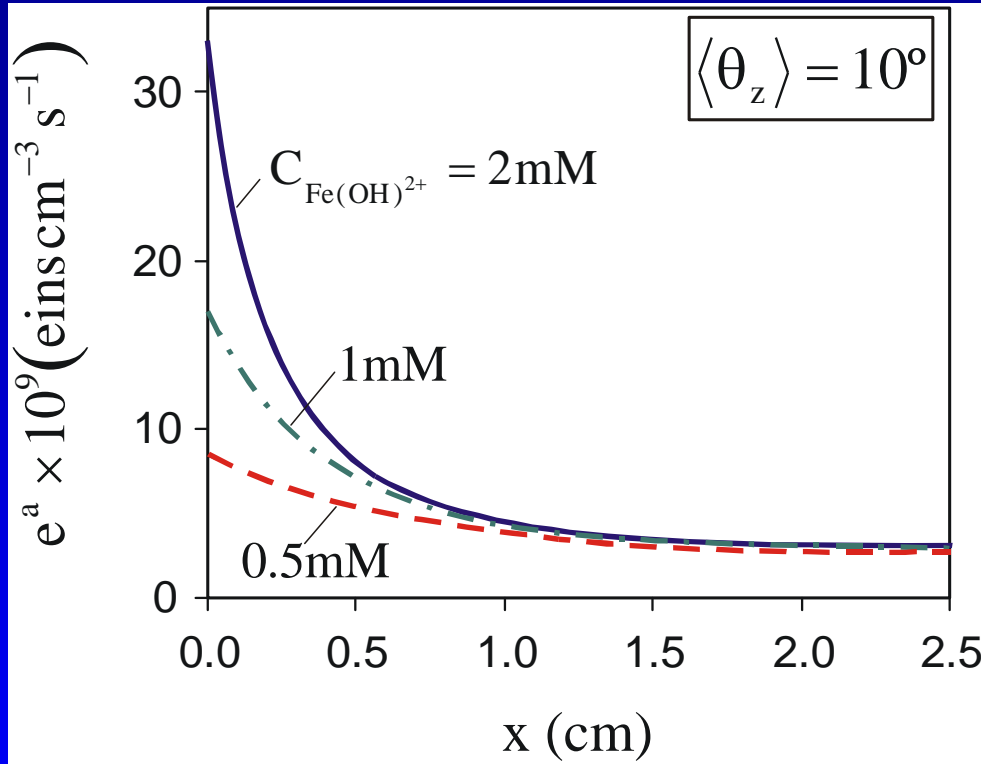


LVRPA as a function of the x-coordinate for:

- × Three different zenith angles: 10° , 30° , 60°
- × Constant absorbing species concentration: $C_{\text{Fe(OH)}^{2+}} = 1 \text{ mM}$

→ As expected, the radiation field along the x-coordinate is highly non-uniform: $e^a(x = 0.5 \text{ L}) \cong 0.2 e^a(x = 0)$

PREDICTIONS OF THE LVRPA

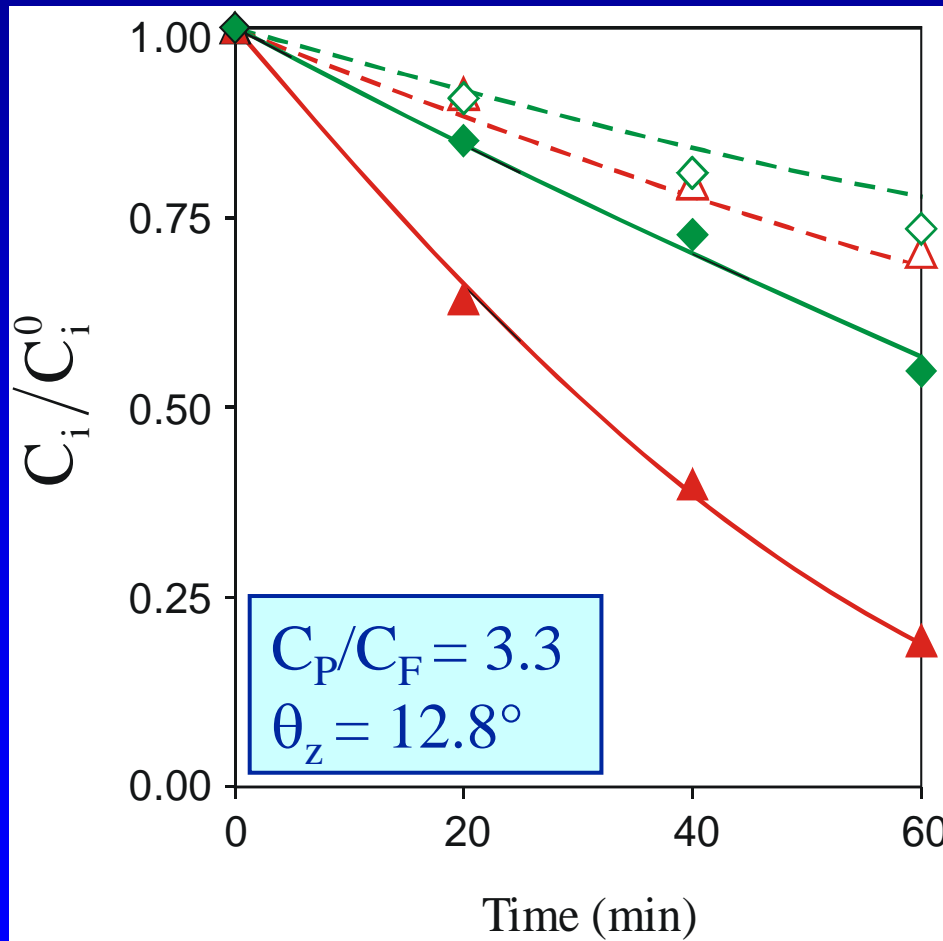


e^a as a function of the x-coordinate for:

- × three different ferric ion concentrations:
 $C_{\text{Fe(OH)}^{2+}} = 0.5, 1, 2 \text{ mM}$
- × a constant solar zenith angle: $\theta_z = 10^\circ$

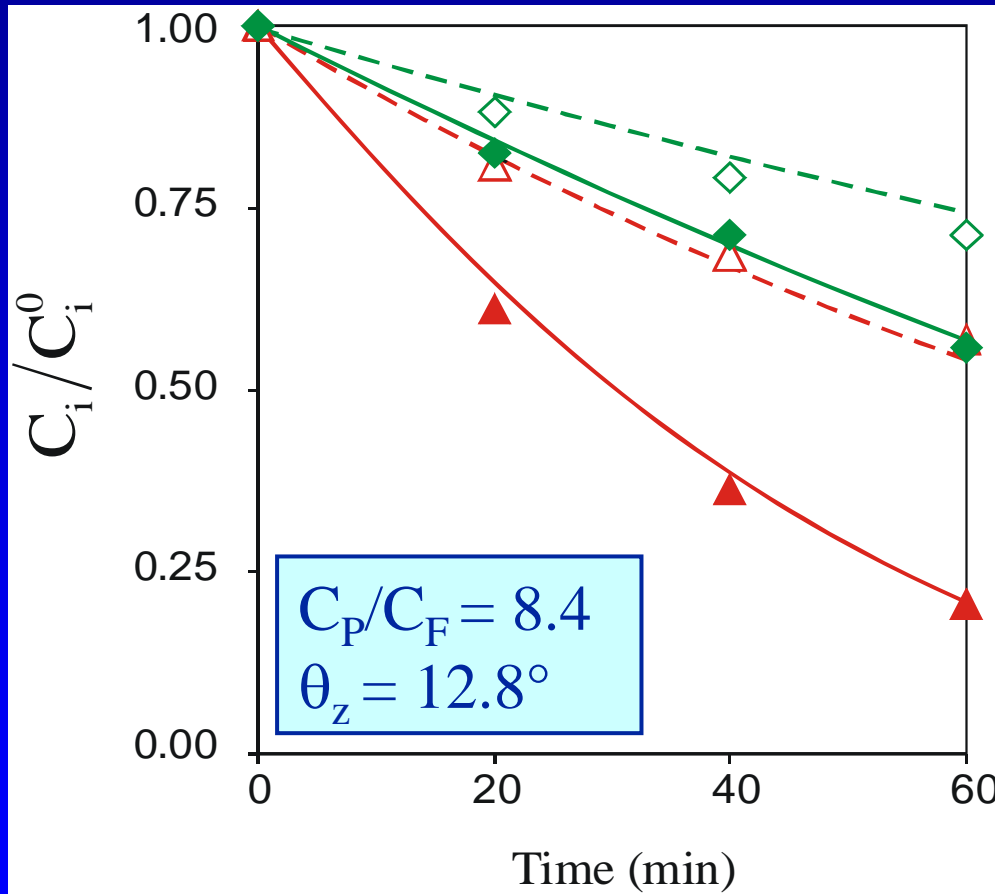
→ When the optical density is increased the shape of the LVRPA curve becomes steeper

PREDICTED AND EXPERIMENTAL RESULTS (T = 25 °C)



- × Model predictions and experimental data as a function of time
- × Formic acid relative concentration:
 - Fenton (- - -)
 - photo-Fenton (—)
- × H_2O_2 relative concentration:
 - Fenton (- - -)
 - photo-Fenton (—)

PREDICTED AND EXPERIMENTAL RESULTS (25 °C)



- × A similar representation is shown for a higher C_P/C_F
- × Conversion for the photo-Fenton reaction is always higher than that obtained with the Fenton reaction
- × Model and experimental results show good agreement
- × The maximum error is 9%

COMPARISON BETWEEN FENTON AND PHOTO-FENTON CONVERSIONS (25 °C)

	C_P/C_F	Pollutant conversion (%)				Conversion Enhanc.(%)
		Fenton $\epsilon(\%)$	photo-Fenton $\epsilon(\%)$			
Exp. Data	3.3	29.3	-	80.7	-	175.4
Predictions	3.3	31.1	6.1	81.0	0.4	160.4
Exp. Data	5.4	37.6	-	80.6	-	114.4
Predictions	5.4	39.7	5.6	80.2	0.5	102.0
Exp. Data	8.4	43.2	-	79.3	-	83.6
Predictions	8.4	45.7	5.8	78.6	0.9	72.0

- × A conversion of 81% has been achieved for the lowest C_P/C_F
- × The photo-Fenton system produces a conversion up to 175% greater than that obtained with the Fenton reaction ($C_P/C_F=3.3$)

COMPARISON BETWEEN FENTON AND PHOTO-FENTON CONVERSIONS (25 °C)

	C_P/C_F	Pollutant conversion (%)				Conversion Enhanc.(%)
		Fenton ϵ (%)	photo-Fenton ϵ (%)			
Exp. Data	3.3	29.3	-	80.7	-	175.4
Predictions	3.3	31.1	6.1	81.0	0.4	160.4
Exp. Data	5.4	37.6	-	80.6	-	114.4
Predictions	5.4	39.7	5.6	80.2	0.5	102.0
Exp. Data	8.4	43.2	-	79.3	-	83.6
Predictions	8.4	45.7	5.8	78.6	0.9	72.0

Notice that the photo-Fenton conversion decreases when the C_P/C_F initial molar ratio is increased.

EFFECTS OF THE H₂O₂ ON FORMIC ACID CONVERSION (T = 25 °C)

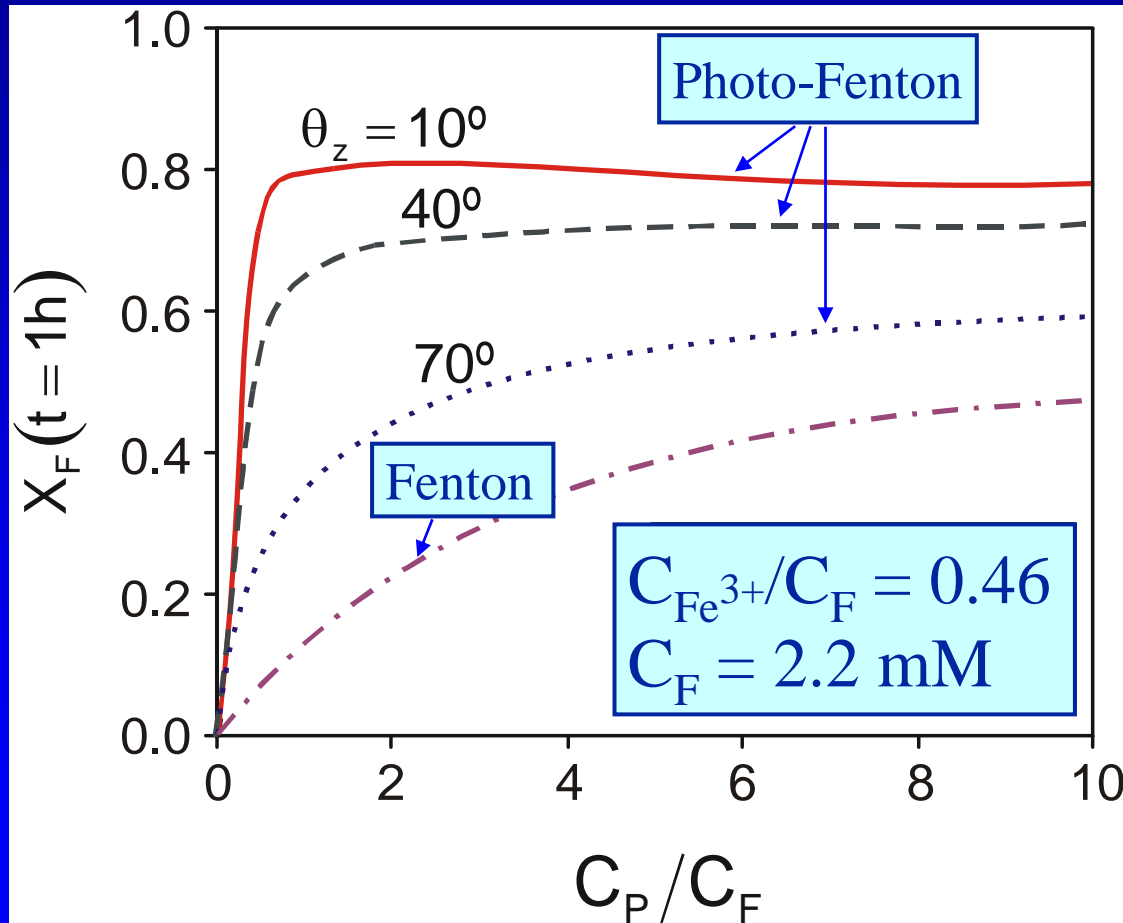
The change in the H₂O₂ concentration (C_p) may have two opposite effects:

- × At low C_p, ferrous ion (Fe²⁺) generation may be too low and so will be the OH• generation.
- × At high C_p, H₂O₂ acts as a radical trapping agent, thus competing with the pollutant degradation path and rendering lower degradation rates:



- × Thus, an optimal molar ratio C_p/C_F should be expected.

PARAMETRIC STUDY: EFFECTS OF THE H_2O_2 ON FORMIC ACID CONVERSION



$X_F(t = 1\text{ h})$ vs. C_P/C_F :

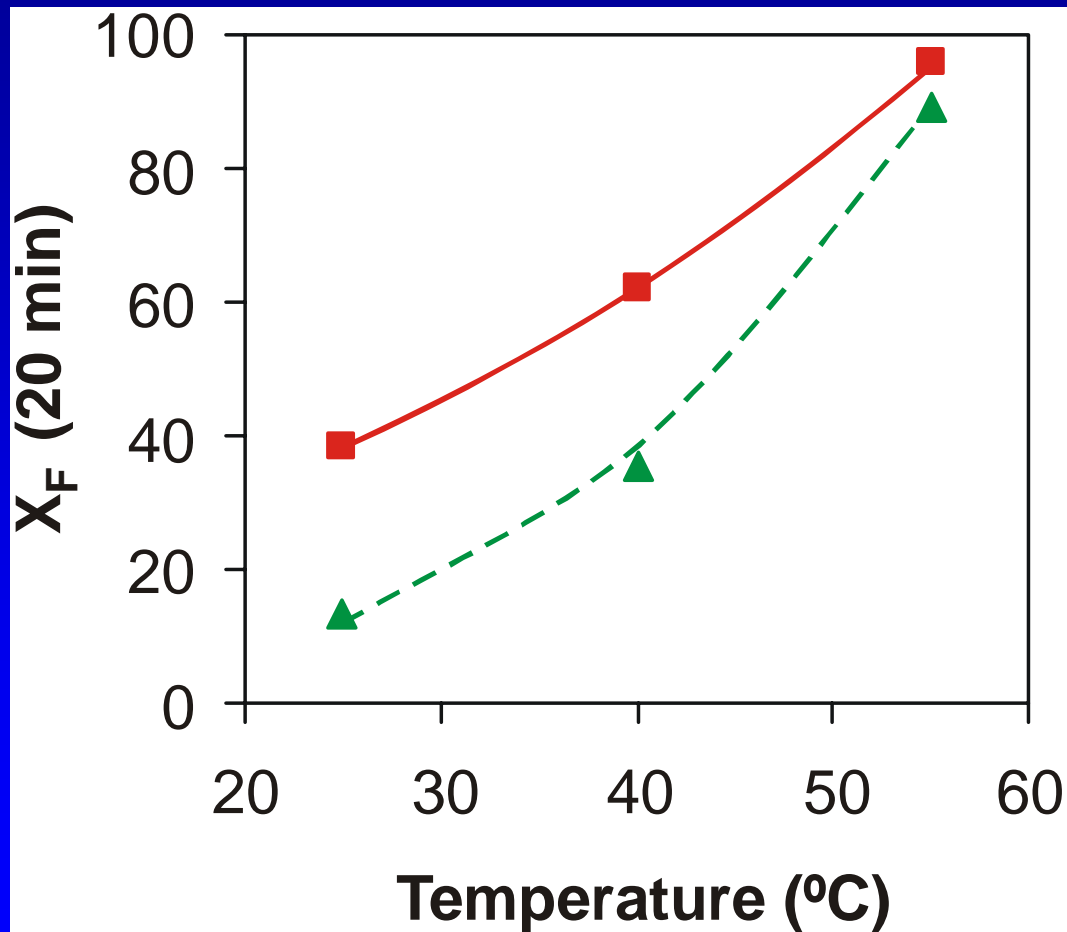
◆ Fenton and ph-Fenton

◆ $\theta_Z = 10^\circ, 40^\circ, 70^\circ$

⊆ At high values of θ_Z , increasing the C_P/C_F ratio increases the conversion

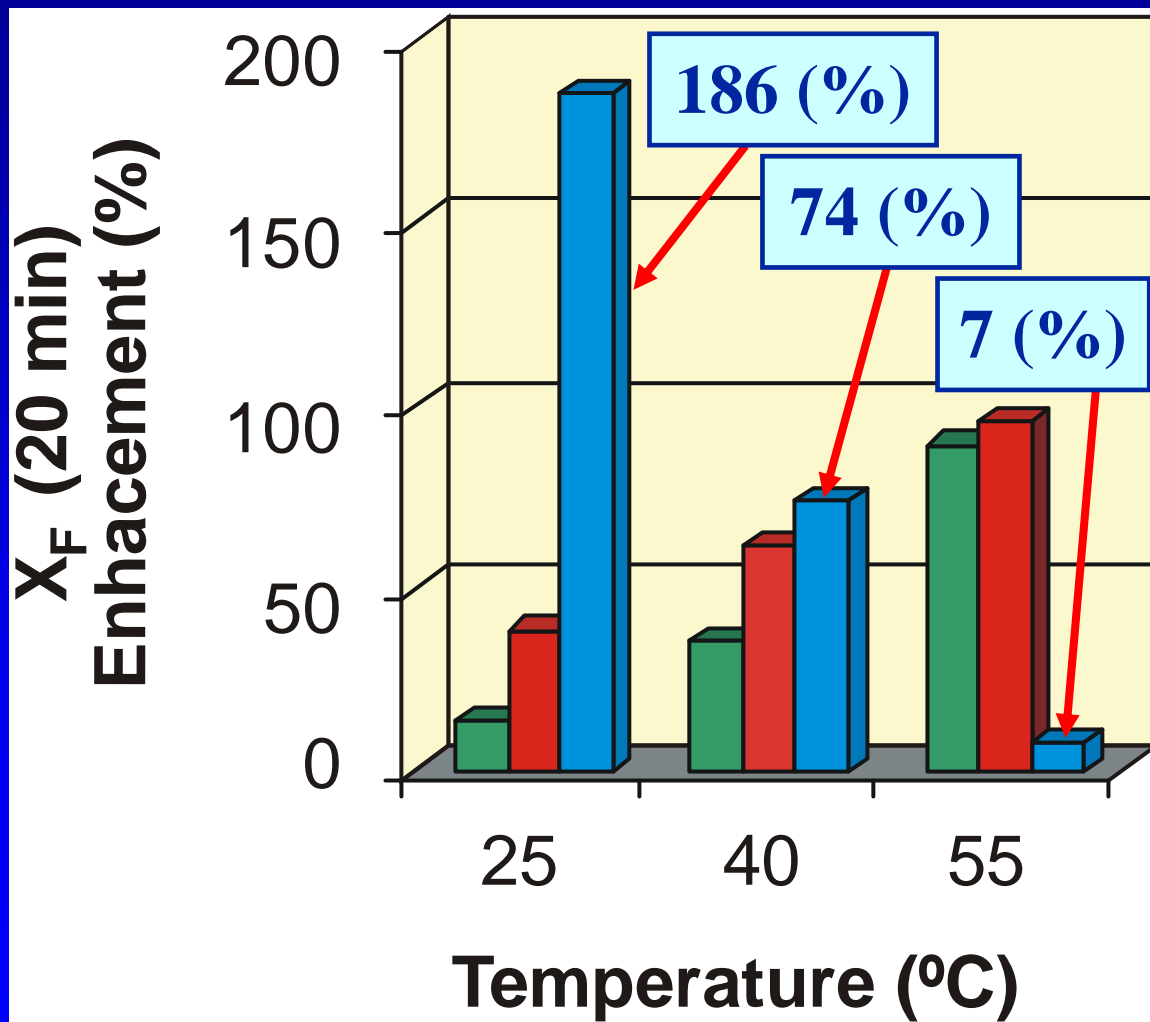
⊆ At low values of θ_Z (high radiation), an optimal molar ratio C_P/C_F is observed

COMPARISON BETWEEN FENTON AND PHOTO-FENTON CONVERSIONS (t = 20 min)



- × Model predictions of formic acid conversion:
 - Fenton (— —)
 - photo-Fenton (—)
- × Experimental data:
 - Fenton (▽)
 - photo-Fenton (■)
- × Increasing the reaction temperature decreases the enhancement of the pollutant conversion

POLLUTANT CONVERSION AND CONVERSION ENHANCEMENT (t = 20 min)



- × UV solar radiation improves the effectiveness of the Fenton process
- × For the lowest temperature 25°C, the pollutant conversion is significantly increased
- × Intermediate behavior for 40°C
- × For the highest temperature 55°C, this effect is less important

FINAL REMARKS

- ✓ Increased reaction temperature can enhance the reaction rate of the Fenton and photo-Fenton processes.
- ✓ However, at higher temperatures: (i) this conversion enhancement is less important and (ii) the efficiency of hydrogen peroxide declines: decomposition of H_2O_2 into oxygen and water (Malik and Saha, 2003).
- ✓ It is possible to take advantage of the natural temperature of a wastewater at the end of the process (in the textil industry: Rodríguez et al., 2002).
- ✓ Possibility of a combined photochemically and thermally enhanced Fenton process, using solar energy (UV/Vis + IR photons: Sagawe et al., 2001).

THANKS

- x Dr. Rubén D. Piacentini, Grupo de Energía Solar, Instituto de Física Rosario (IFIR), Rosario - Argentina
- x UNIVERSIDAD NACIONAL DEL LITORAL (UNL) (National University of Litoral, Santa Fe - Argentina)
- x CONSEJO NACIONAL DE INVESTIGACIONES CIENTIFICAS Y TECNICAS (CONICET) (National Council for Science and Technology of Argentina)
- x AGENCIA NACIONAL DE PROMOCION CIENTIFICA Y TECNOLOGICA (ANPCYT) (National Agency for the Promotion of Science and Technology of Argentina)